SOME ASPECTS OF GYRO-SPLITTING IN THE IONOSPHERE

By G. G. Bowman*

[*Manuscript received October* 4, 1961]

Summary

Ionograms for Hobart (geomagnetic latitude 52 °S.), showing x-mode propagation below the electron gyro frequency, were examined. Detailed analyses of some ionograms were made. Strong reflections for this particular propagation seem dependent on the amount of ionization, between the sporadic E level and 180 km, being reduced to a sufficiently low value. It is suggested that this can be achieved, in the sporadic E region, by the concentration of existing ionization; this concentration producing the sporadic E reflections.

I. Introduction

Ionograms with traces above the F trace which, starting at the lowest frequencies, show increasing retardation as the electron gyro frequency is approached, have been reported in the literature for over 20 years. Several attempts have been made to explain these traces. The most plausible, in the light of present knowledge, seems to be that put forward by Appleton, Farmer, and Ratcliffe (1938). They proposed that the echo results from propagation in the x-mode, radiation being returned to the sender after reflection at the $X=1+Y$ level. To distinguish such echoes from x-ray echoes above the gyro frequency, they will be referred to hereunder as x_G-rays.

Some of the earlier controversies are recorded by Martyn and Munro (1939). One example of these is the doubt which existed regarding the location of the retarding region. Some multiple-hop traces of this echo (e.g. $2F_2-E_s$) were reported showing no increase in retardation on that shown by the first hop; indicating a retarding region between the ground and the sporadic E layer. However, the $1F_2+E_s$ trace also showed similar retardation to that for the $1F_2$ trace, giving evidence against a retarding region below the sporadic E layer.

Ellis (1960) has explained this apparent discrepancy by postulating that, in some cases, the radiation travels for part of its path in the o-mode and part in the x-mode, the transition occurring by coupling during reflection from the upper side of the E_s layer. Ellis suggests that the retardation always occurs between the E_s and F_2 layers.

The present paper is principally concerned with a detailed study of a few individual cases in the light of Ellis's theory. This study confirms his interpretation and sheds some light on the ion density near the E_s reflection level, and between this and the F_2-layer reflection level, in the pre-daylight hours; and the relation between these and ionospheric irregularities at both reflection levels.

* Physics Department, University of Queensland, Brisbane.

II. Diurnal, Seasonal, and Latitude Variation of Occurrence

Five months' records (July to December inclusive, except October, 1946) for Hobart (geomagnetic latitude 52 °S.) have been examined to determine the diurnal and seasonal variations of x_G-rays. A trace of any length (whether it be a weak trace in the vicinity of 1 Mc/s, or a strong one recording frequencies up to values near the gyro frequency) was recorded as an occurrence. Figure 1 (*a*) gives the diurnal variation, indicating a night-time phenomenon occurring between the hours of 2200 and 0700 local time, with a single well-defined maximum at 0200 hr. The seasonal variation (Fig. 1 (*b*)) shows a winter maximum and a summer minimum.

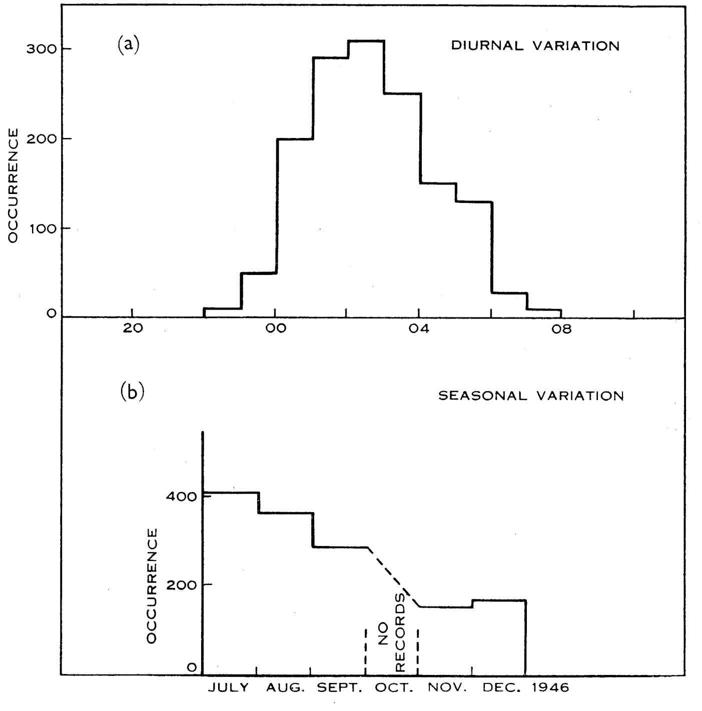

Fig. 1 (*a*).—Diurnal variation of x_G-ray occurrence at Hobart for 5 months of 1946.
Fig. 1 (*b*).—Seasonal variation of x_G-rays at Hobart during 1946.

x_G-Rays are very seldom seen at Brisbane (geomagnetic latitude 35 °S.). However, Figure 4 of Plate 3 shows the ionogram on one occasion when they were observed at this station.

III. Multiplicity of x_G-Rays

If coupling can occur when reflection takes place in the E_s layer, then two possibilities exist in the case of the $2F_2$—E_s echo (Fig. 2 (*a*)). The radiation can pass between the E_s layer and the F_2 reflecting point in the x-mode either once or twice, depending on whether or not coupling takes place. This is also true in the case of the paths equivalent to $2F_2$ reflection shown in Figure 2 (*b*).

In the case of $3F_2-2E_s$ echoes, when there are two reflections from the top side of the sporadic E layer, three possibilities exist; and, in general, if there are n reflection points on the top E_s surface, there will be $n+1$ traces possible for the x_G-ray, all spaced from one another by equal intervals of group path at each frequency.

Figure 3 (*a*) is a tracing of the x_G-rays recorded at Hobart at 0200 on August 3, 1946 (see Fig. 2 of Plate 1 for the actual ionogram). Each of these traces is

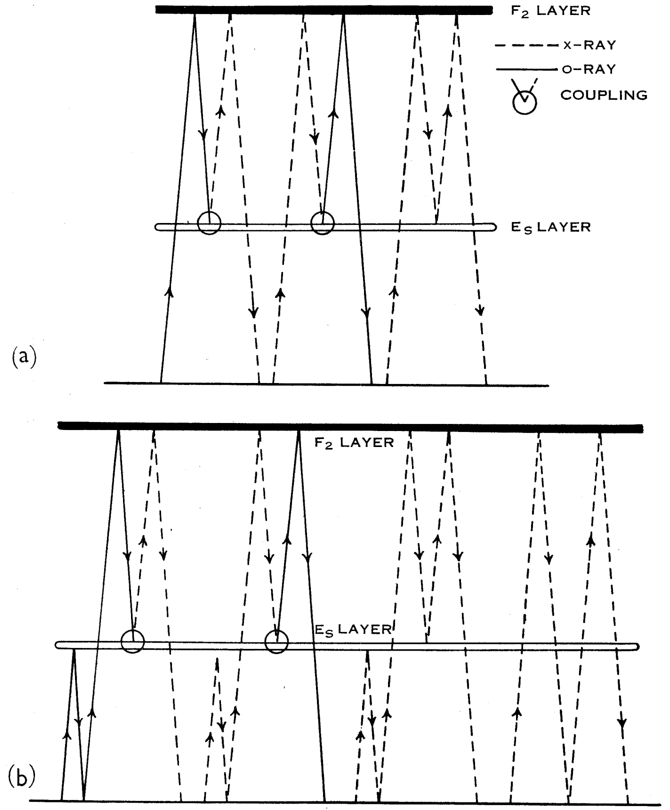

Fig. 2 (*a*).—Possible ray paths for $2F_2-1E_sx_G$-ray traces when coupling is considered.
Fig. 2 (*b*).—Possible ray paths for $2F_2x_G$-ray traces when coupling is considered.

related to a particular type of *o*-ray reflection. For each type of reflection, Figure 3 shows the expected number of x_G-rays. Similar results were obtained in a number (about 50) of other cases examined.

IV. E-Region Ion Densities

Some information concerning ion densities near the E_s reflection level can be deduced from ionograms showing a complete set of x_G-ray traces, visible even close to the gyro frequency, because of the sensitivity of x_G-ray traces to small changes in ion density.

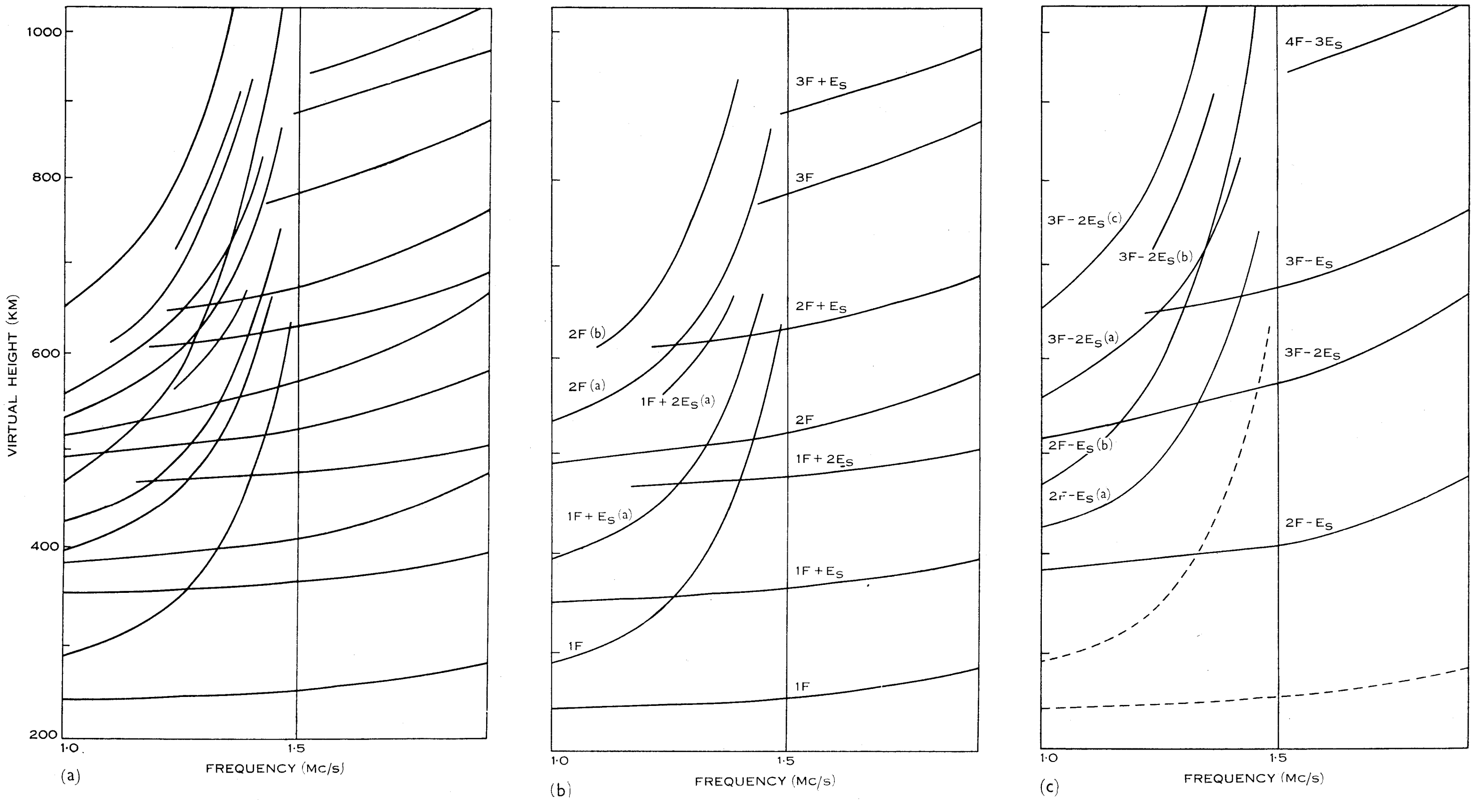

Fig. 3 (a).—Drawing of x_G-ray traces occurring on Hobart ionogram at 0200 on August 3, 1946 (Plate 1, Fig. 2).
Fig. 3 (b).—x_G-Ray traces from Figure 3 (a) associated with $1F_2$, $1F_2+1E_s$, $1F_2+2E_s$, and $2F_2$ modes of propagation.
Fig. 3 (c).—x_G-Ray traces from Figure 3 (a) associated with $2F_2-1E_s$ and $3F_2-2E_s$ modes of propagation.

Figures 4 (*a*) and 4 (*b*) indicate how, by comparison of $1F_2$ with $1F_2+E_s$ and by comparison of $2F_2$ with $2F_2-E_s$, respectively, group paths for *o*-rays and x_G-rays to the bottom and top respectively of the E_s layer can be computed. In Figure 4 (*c*) results obtained in this way from the ionogram reproduced in Figure 3 are plotted.

If, as usual, f_N represents the plasma frequency, f_H the gyro frequency, and f the operating frequency, then we can denote f_N^2/f^2 by X, f_H/f by Y, and the group

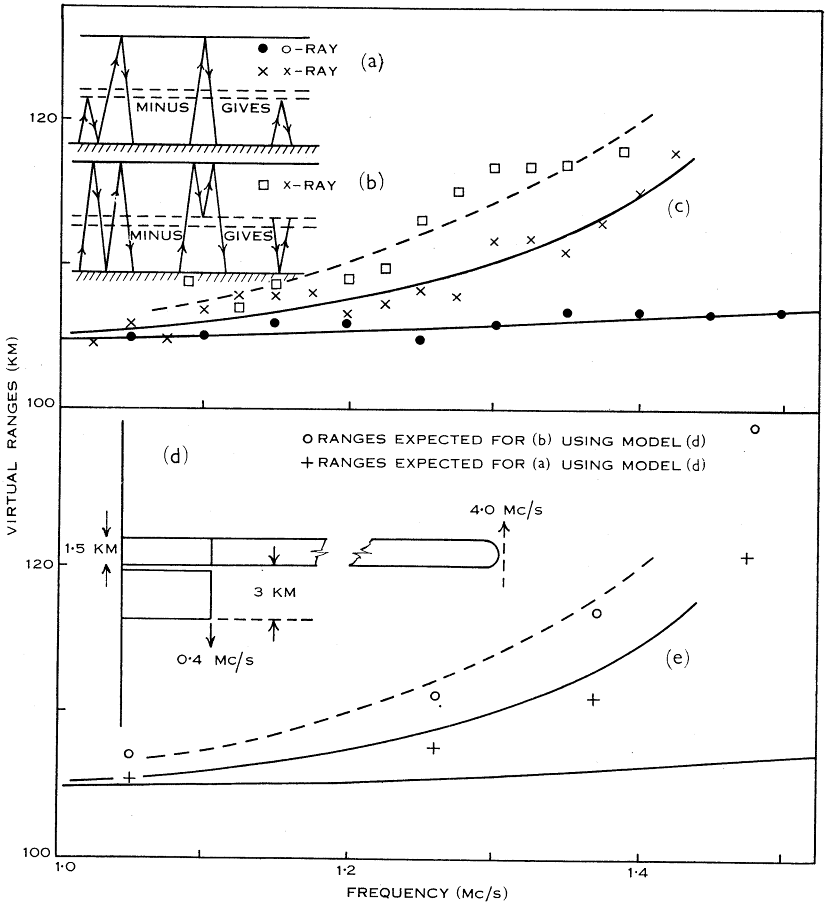

Fig. 4 (*a*).—Method of calculating group paths from ground to under-surface of E_s layers for *o*-rays and x_G-rays.

Fig. 4 (*b*).—Method of calculating group paths from ground to top-surface of E_s layer for x_G-rays.

Fig. 4 (*c*).—Points calculated by methods illustrated in Figure 4 (*a*) and Figure 4 (*b*) from ionogram shown in Plate 1, Figure 2.

Fig. 4 (*d*).—Proposed model of ionization distribution for radiation reflected below the E_s layer and radiation passing through the E_s layer, from the results of Figure 4 (*c*).

Fig. 4 (*e*).—Calculated group paths using model of Figure 4 (*d*) for radiation reflected from, and passing through the sporadic E layer, compared with the observed results (Fig. 4 (*c*)).

refractive index μ' can be computed as a function of $X/(1+Y)$ for a series of values of Y, for the dip angle of Hobart. The Y values chosen correspond, for Hobart ($f_H=1\cdot5$ Mc/s at 230 km), to $f=1\cdot0$, $1\cdot2$, $1\cdot3$, $1\cdot4$ Mc/s and infinity. Curves for these values are shown in Figure 5.

For the calculations of ranges to the under-surface of the E_s layer, it is assumed that retardation in the virtual height recorded for the o-ray is zero, and therefore the extra virtual range for the x_G-ray will be due to ionization below the level of reflection. If the amount of ionization below the reflection level is taken as a block 3 km thick, with a plasma frequency of $0\cdot4$ Mc/s, then Figure 4 (*e*) shows the x_G-ray virtual ranges (plotted as crosses) expected at several frequencies. (The additional retardation was obtained by evaluating $\int(\mu'-1)dh$ from the curves of Fig. 5.) These calculated values give reasonable agreement with the best line through the observed values of Figure 4 (*c*).

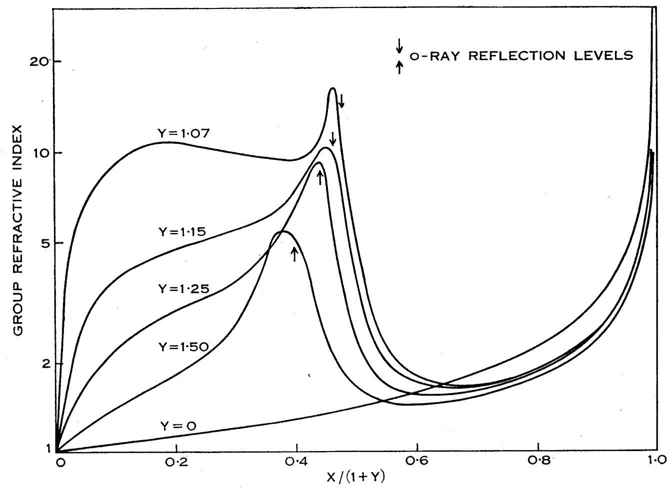

Fig. 5.—Plots of group refractive indices (μ') against $X/(1+Y)$ for various values of Y for Hobart (geomagnetic latitude 52 °S.).

The exact nature of ion distribution in the sporadic E layer is not known. An extremely thin layer would give partial transmission of incident radiation. On the other hand transmission through the sporadic E region can also occur if the ion density comprising the sporadic E layer is patchy ; the radiation passing between the concentrations.

Assuming the latter hypothesis to be true, it has been possible, from the retardations calculated for passage through the layer, to make an estimate of the background ionization encountered by the penetrating radiation.

A block of ion density, of plasma frequency $0\cdot4$ Mc/s and $1\frac{1}{2}$ km thick, will give, when taken with the estimated ionization below the layer, virtual ranges from the ground to the top of the E_s layer (circles in Fig. 4 (*e*)) which are comparable with those observed (Fig. 4 (*c*)).

This model gives an ion content from the ground to the top of the E_s layer of $9\cdot0\times10^8$ cm^{-2}.

V. Ion Densities below the F_2 Region

A method of $N(h)$ profile analysis, due to Titheridge (1959*a*), allows an estimation of the electron content between the E_s layer and the F_2 layer, and from this a density profile of the lower part of the F_2 layer can be estimated. It was thought that calculation of such a profile at the time of a particular x_G-ray occurrence would give a reasonably good model with which to work. For ionograms similar to those used in this analysis the method does not give the exact shape of the electron distribution below the reflection level of the lowest recorded frequency (1 Mc/s). Titheridge assumes a linear decrease of ion density with decrease in height for this region of the $N(h)$ profile.

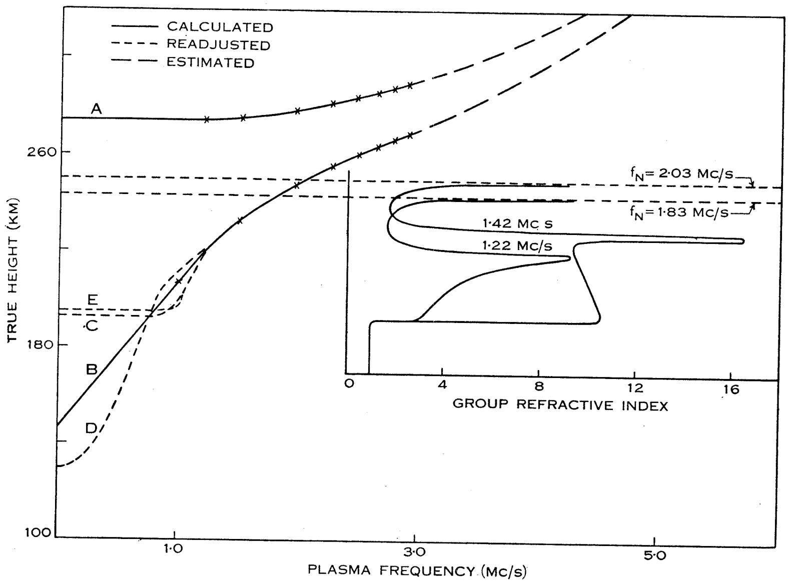

Fig. 6.—Various models of F_2 layer ionization distribution for Hobart at 0210 on September 27, 1946. The variations of μ' with height for model C (for 1·22 and 1·42 Mc/s) are also shown.

Figure 6 shows $N(h)$ profiles calculated for Hobart from the ionogram taken at 0210 on September 27, 1946 (Fig. 4 of Plate 1). Line A represents the $N(h)$ profile calculated from the *o*-ray alone, which does not allow for the ionization between the layers, while line B gives that calculated by the Titheridge method. Using this model, the group path expected for the x_G-ray at various frequencies (by evaluating $\int \mu' dh$) was calculated and the resulting curve was then compared with observations. A close fit was not obtained.

Titheridge's assumption of linear decrease of ion density in the lower part of the F_2 layer is, however, arbitrary. The assumed shape of the profile can therefore be changed, provided the total electron content is not thereby altered. Trial and error methods were then adopted to determine the profile which gave the best results. This was obtained by model C on Figure 6. The calculated points can be compared with the observed trace in Figure 7 (a). Also shown on Figure 7 (a) are the curves obtained by using models B and D respectively.

If one assumes, on this occasion, the ion density encountered by radiation transmitted through the sporadic E region to be comparable with that found in Section IV (say 5 km depth of plasma frequency 0·4 Mc/s), then calculation will give line E for the best fit. This is almost the same as the profile indicated by line C.

Similar calculations of $N(h)$ profiles for ionograms at 0110 on September 18, 1946 and at 0200 on August 3, 1946 (Plates 2 and 1 respectively) have been made, and these are shown in Figure 8. On all three occasions the estimates

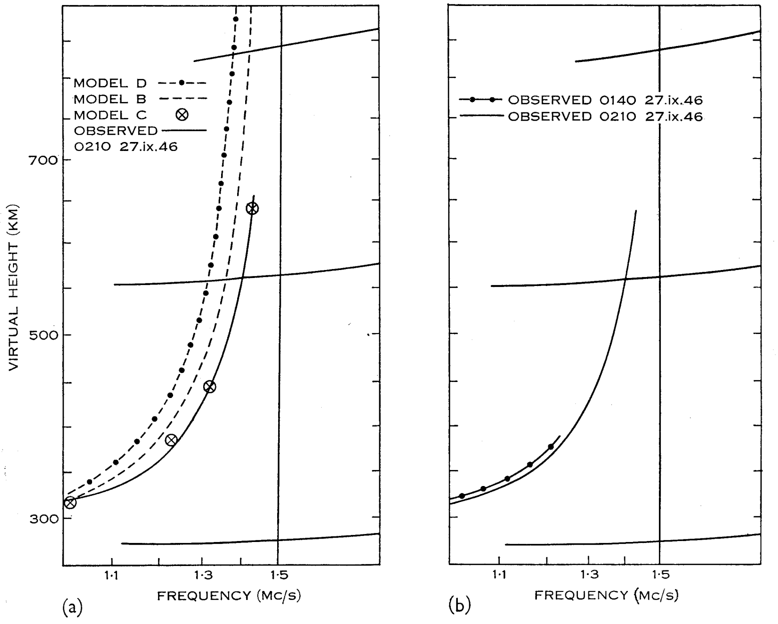

Fig. 7 (a).—Calculated group paths for x_G-rays using models of Figure 6, compared with observed trace.

Fig. 7 (b).—Observed x_G-ray traces at 0140 and 0210 on September 27, 1946 (Hobart).

suggest that the F_2-layer ionization drops rapidly at a relatively high level (above 180 km). This suggests that such an ion density distribution is a necessary condition for strong x_G-rays. Possible reasons for this will be discussed later.

The high sensitivity of the x_G-ray virtual ranges to the distribution of electrons between the E_s layer and the F_2 layer becomes apparent if one considers the estimated virtual paths at 1·42 Mc/s for the three models marked C, B, and D on Figure 6. Estimated values (ignoring the anticipated small region of enhanced electron density through which the radiation passes at the sporadic E level) are as follows: model C, 640 km; model B, 850 km; model D, 10,200 km. The observed value on this occasion was 630 km. This suggests that the electron content between the layers must be very low; otherwise retardation produced for frequencies near the gyro frequency (e.g. 1·42 Mc/s) will give a virtual range much greater than that observed. Of course, a sharp rise of electron density shown by model C is not physically possible. However, a slight modification of model C to remove this objection will not change the argument.

An estimate of the upper limit of ion density in the region between the E_s layer and the base of the F_2 layer can be obtained by calculating the additional retardation contributed by certain uniform densities in this region. For a density with a plasma frequency of 0·2 Mc/s the extra retardation for a frequency of 1·42 Mc/s (x-mode considered) would be approximately 200 km; while for a plasma frequency of 0·1 Mc/s the extra retardation would be approximately 50 km. An ion density with a plasma frequency somewhat less than 0·1 Mc/s is indicated. Rocket results for high latitude stations (Ratcliffe 1960) have shown that, at times, the region being considered can have very little ion content.

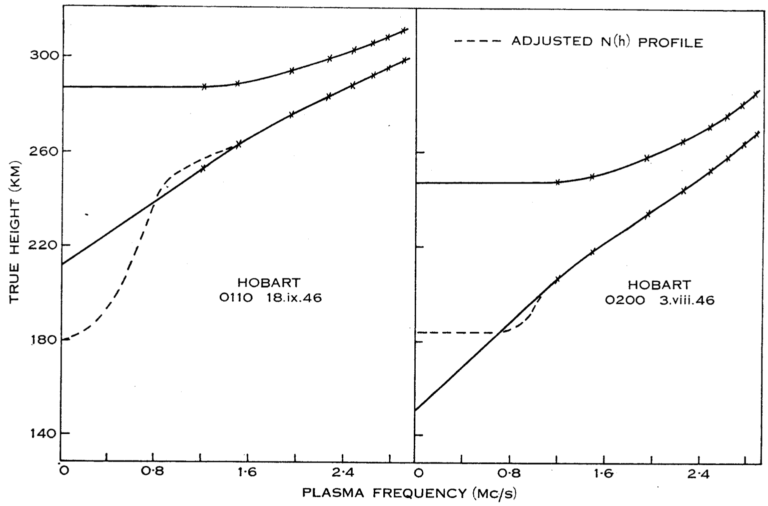

Fig. 8.—Calculated $N(h)$ profiles at Hobart for 0110 on September 18, 1946, and at 0200 on August 3, 1946, after making allowance for x_G-ray trace shapes.

The positions in the layer where the principal contributions to retardation occur can be seen from Figure 6. Figure 5 shows that the value of μ' (for the x-ray below the gyro frequency) has a maximum at the o-ray reflection level for the particular frequency being considered. At the lower frequencies involved in this investigation (around 1 Mc/s) most of the retardation experienced by the x_G-ray comes from this o-ray reflection level (see Fig. 6 for the variation of μ' with height for 1·22 Mc/s). However, Figure 5 predicts and Figure 6 shows (cf. 1·42 Mc/s *v.* 1·22 Mc/s curve) that, as the electron gyro frequency is approached, the contributions to the retardation of regions of lower ionization density become relatively more important.

VI. Ionospheric Irregularities and x_G-Rays

Examination of ionograms from Hobart showing x_G-rays reveals that their occurrence is sporadic. On any one night strong x_G-rays may come and go several times. Plate 2 shows an isolated occurrence of relatively strong x_G-rays. These, and x_G-rays recorded on other occasions, suggest a possible association between x_G-rays and sporadic E. This has been pointed out by Ellis (1960) and is the subject of Section VII of this paper.

On occasions, prior to the onset of a period of enhanced x_G-rays, a strong x_G-ray trace will appear in the $3F_2-2E_s$ hop mode, while the $1F_2$ x_G-ray trace is weak or missing. The ionograms for 0040 on August 3, 1946 (Fig. 1 of Plate 1), and for 0030 on September 18, 1946 (Plate 2) illustrate this strong $3F_2-2E_s$ x_G-ray trace.

$N(h)$ profiles have been calculated from ionograms (0200 until 0140 inclusive) on September 18, 1946 (Plate 2) by a method proposed by Titheridge (1959a) (see Section V). From these profiles it was possible to deduce the height-time

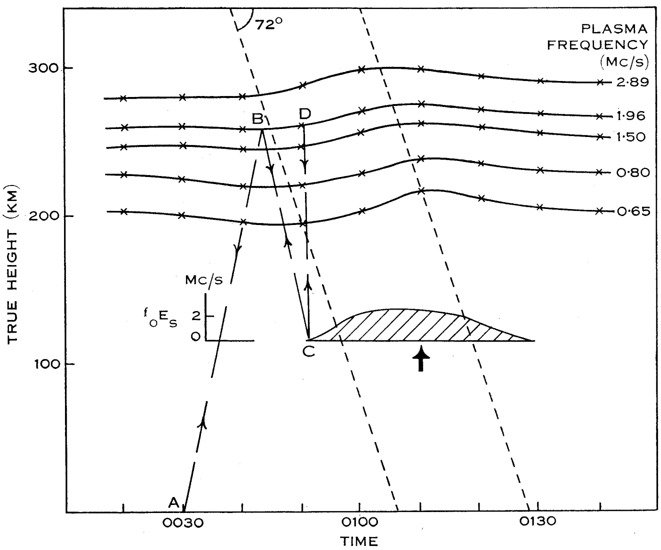

Fig. 9.—Ionization contours drawn from $N(h)$ profiles from 0020 until 0140 (inclusive) for Hobart on September 18, 1946. f_0E_s values and a proposed $3F_2-2E_sx_G$-ray path are also shown.

variation of several contours of equal ionization (Fig. 9). An F_2-layer irregularity results, which has the characteristics of those described previously (Bowman 1960a). The presence of a third magneto-ionic component (z-ray) at 0050 and 0100 suggests that the ripple irregularity extends in an east-west direction (Bowman 1960c). Also, previous work (Bowman 1960a) has shown that, in such a case, the sloping front of the irregularity should lie along the direction of the Earth's magnetic field. If now the time scale is adjusted so that the irregularity has a slope in this direction, the vertical and horizontal scales should be the same. This has been done in Figure 9.

The variation of f_0E_s, while the range remains constant, is also plotted on Figure 9. The sporadic E occurrence appears associated with the F_2-layer irregularity (Bowman 1960b); also, the x_G-ray occurrence appears to be most pronounced when f_0E_s is maximal.

A ray path for a $3F_2-2E_s$ echo, involving reflection from the top front-edge of the sporadic E patch, is indicated on Figure 9. Since the x_G-ray for this path shows retardation representing only one return E_s-layer/F_2-layer passage in the x-mode, coupling must occur at point C on two occasions. This gives the path CDC where the radiation propagates in the x-mode.

Traces are also recorded as satellites to the x_G-rays, in the same way as they are recorded at frequencies above the gyro frequency (Bowman 1960*a*). Plate 3, Figures 1, 2, and 3, shows satellite traces from ionospheric irregularities, similar to those constituting the " spread-F " traces at the higher frequencies of the ionograms.

VII. x_G-Ray Intensity and E_s Reflectivity

The observations made in Section IV give an estimation of the ionization encountered by an x_G-ray in passing " through " a region where sporadic E is present. Ellis (1960) has shown that, on most occasions when x_G-rays are recorded at frequencies close to the gyro frequency, sporadic E is also recorded with a critical frequency between 3 and 4 Mc/s.

A comparison has been made of the shape of fragmentary x_G-ray traces appearing before, or after, such periods of good reflection, with the shape of the complete traces. Thus Figure 7 (*b*) shows the retardations for the two traces, spaced in time by an interval of 30 min, shown in Figures 3 and 4 on Plate 1. The fragmentary trace, present before the sporadic E occurrence, is seen from Figure 7 (*b*) to show slightly greater retardation than the later complete trace. This slightly greater retardation for the weak trace was always observed when two ionograms satisfying the above conditions were found. The ionograms for a similar occurrence on August 3, 1946 are shown in Plate 1, Figures 1 and 2. Table 1 is a record of a number of occasions when weak and strong traces have been recorded in near succession, under similar circumstances. For each entry at 1 Mc/s, the retardation of the weak trace exceeds that of the strong one, the average value of this excess being $9 \cdot 3$ km.

The greatly reduced intensity of the fragmentary trace must be due to additional absorption at some level. It seems most unlikely that this could arise from a redistribution in height of the electrons at the base of F_2, for to obtain the required additional absorption it would be necessary to postulate a major redistribution which, as shown in Section V, would produce a drastic change in the shape of the x_G-ray trace. A more likely hypothesis is that the redistribution of electrons and consequent rise in absorption take place in the vicinity of the E level, for, because of the higher collision frequency (by a factor of 100), a less marked redistribution is required to give the necessary rise in absorption.

Calculations have been made using the model deduced from the ionogram at 0210 on September 27, 1946 (model C of Fig. 6).

Using the expression $K=(\nu/2c)(\mu'-\mu)/(1-\frac{1}{2}Y_L)$ (Q.L. approximation for the extraordinary wave, Ratcliffe 1959, p. 132) for the deviative absorption coefficient, $\int K\mathrm{d}h$ has been determined graphically, giving, for a frequency of $1 \cdot 42$ Mc/s, a value of 1 neper. Also, using the expression $K=(\nu/2c)(1/\mu)\{X/(1-Y_L)^2\}$ (Q.L. approximation for the extraordinary wave, Ratcliffe 1959, p. 131) for the non-deviative absorption coefficient, $\int K \mathrm{d}h$ has been determined, for a frequency of 1·42 Mc/s for a distribution of ionization at the sporadic E level, similar to that found for the case analysed in Section IV. Here it has been assumed that the ionization encountered by the x_G-ray, in passing " through " the sporadic E layer, is represented by a slab of ionization 5 km thick, having a density with a plasma frequency of 0·4 Mc/s (see Section IV). The non-deviative absorption in this case gave a value of 4·4 nepers; so the overall absorption (deviative and non-deviative) for the model chosen amounts to 5·4 nepers.

Table 1

WEAK AND STRONG TRACES RECORDED IN NEAR SUCCESSION

Date	Well-defined Traces			Weak Traces			Difference in Retardation (km)
	Time	f_0E_s (Mc/s)	Diff. h' at 1 Mc/s o-Ray and x-Ray (km)	Time	f_0E_s (Mc/s)	Diff. h' at 1 Mc/s o-Ray and x-Ray (km)	
6. vii.46	0510	1·5	47	0600	$<1\cdot0$	57	10
25. vii.46	0300	3·5	55	0410	1·2	60	5
27. vii.46	0210	4·0	50	0250	1·5	60	10
29. vii.46	0310	2·0	60	0230	$<1\cdot0$	73	13
3.viii.46	0100	3·0	38	0040	$<1\cdot0$	50	12
7.viii.46	0350	2·0	45	0300	$<1\cdot0$	60	15
9.viii.46	0110	3·0	45	0100	$<1\cdot0$	55	10
10.viii.46	0310	3·5	30	0250	$<1\cdot0$	40	10
18. ix.46	0110	2·5	60	0030	$<1\cdot0$	63	3
27. ix.46	0210	3·0	50	0140	$<1\cdot0$	55	5
	Average value for difference in retardation						9·3

However, from Figure 7 (b), it can be seen that at 1 Mc/s the x_G-ray virtual height at 0140 (no sporadic E observed) is approximately 5 km greater than that observed at 0210 (f_0E_s=3 Mc/s). Models can now be proposed which will give this variation in retardation. The two ionograms concerned here are suited to this treatment, as the o-ray trace remains unaltered during this period, thus eliminating any complication to the calculation from a change in the F_2-layer distribution. Extra ionization distributions, which will account for the observed result, are listed in Table 2. It is seen, from the other figures presented in Table 2, that extra ionization at the sporadic E level, which accounts for the slight increase in retardation, is effective in increasing the total absorption by a factor of 3 or 4, depending on which model is chosen. The consequences of these calculations will be discussed later in this paper.

The increase in signal strength with the onset of sporadic E apparently is not confined to the x_G-ray. The low frequency tail of the x-ray, above the gyro frequency, on occasions, also indicates increased signal strength at these times of x_G-ray occurrence. A recent paper by Umlauft (1960) also suggests that, at times of moderate sporadic E occurrence, frequencies above the gyro frequency encounter better F_2-layer reflection conditions.

TABLE 2

MODELS TO ACCOUNT FOR EXTRA RETARDATION

Plasma Frequency of Extra Ionization (Mc/s)	Depth (needed) of Extra Ionization (km)	Extra Absorption produced at 1·42 Mc/s (x_G-ray) (nepers)	Total Absorption for Each Model (nepers)
0·4	18·5	16·3	21·7
0·6	8·8	15·3	20·7
0·8	4·6	12·3	17·7

VIII. DISCUSSION

It is possible that focussing effects, due to the appropriate curvature of F_2 ionization contours, may contribute to the variations in intensity of x_G-rays. However, it seems likely that the enhancement of intensity occurs because of the concentration of existing ionization at E level into a compact sporadic E layer, this leading to a reduction in the overall absorption. In favour of this hypothesis is the coincidence between the intensity enhancements and the appearance of E_s reflections at relatively high frequencies regardless of the shape of F_2 ionization contours at the time.

The average $N(h)$ profiles for Slough (dip 67°) and Watheroo (dip 64°), determined by Titheridge (1959*b*), indicate that the ion density between the E_s layer and the F_2 layer is lowest at around 0200, and hence less absorption of the x_G-ray occurs than at other times. This is consistent with the observations shown in Figure 1, which indicate that x_G-ray traces are most frequently recorded at this time of night, and with the conclusion (Section V) that the ion density below 180 km was quite low during the individual x_G-ray occurrences examined in detail.

In the same way the much more frequent occurrence of x_G-rays at Hobart than at Brisbane can be explained by the generally higher level of ionization above Brisbane and hence greater absorption in the important 100–180 km region.

The enhancement of the $3F_2-2E_s$ x_G-ray shown in Plate 2, at a time when no other x_G-ray appears, can be explained on the basis of the picture represented in Figure 9, if it is assumed that, because of the compression of the ionization between 100 and 180 km in that part of the ionosphere which gives strong E_s reflections, the absorption along the path CDC is relatively weak. The retardation is consistent with the supposition that it is only in this part of the path that the radiation is propagated in the x-mode.

IX. Acknowledgments

The author would like to thank Professor H. C. Webster for his assistance in the preparation of this paper. Thanks are also due to the Ionospheric Prediction Service, which made available the ionograms used in this analysis.

X. References

Appleton, E. V., Farmer, F. T., and Ratcliffe, J. A. (1938).—*Nature* **141**: 409.

Bowman, G. G. (1960*a*).—*Planet. Space Sci.* **2**: 133.

Bowman, G. G. (1960*b*).—*Planet. Space Sci.* **2**: 195.

Bowman, G. G. (1960*c*).—*Planet. Space Sci.* **2**: 214.

Ellis, G. R. A. (1960).—*J. Atmos. Terr. Phys.* **18**: 20.

Martyn, D. F., and Munro, G. (1939).—*Terr. Magn. Atmos. Elect.* **44**: 1.

Ratcliffe, J. A. (1959).—"The Magneto-ionic Theory and its Applications to the Ionosphere." (Cambridge Univ. Press.)

Ratcliffe, J. A. (1960).—"Physics of the Upper Atmosphere." (Academic Press: London.)

Titheridge, J. E. (1959*a*).—*J. Atmos. Terr. Phys.* **17**: 110.

Titheridge, J. E. (1959*b*).—*J. Atmos. Terr. Phys.* **17**: 126.

Umlauft, G. (1960).—*J. Atmos. Terr. Phys.* **18**: 253.

Explanation of Plates 1–3

Plate 1

Fig. 1.—Ionogram (Hobart, 0040, 3.viii.46) showing strong $3F_2-2E_s x_G$-ray trace recorded prior to multiple occurrence of x_G-ray traces.

Fig. 2.—Ionogram (Hobart, 0200, 3.viii.46) showing strong x_G-rays related to the various hop modes, coincident with strong E_s reflections.

Fig. 3.—Ionogram (Hobart, 0140, 27.ix.46) showing weak x_G-ray 30 min prior to strong x_G-ray at 0210 (Fig. 4, Plate 1).

Fig. 4.—Ionogram (Hobart, 0210, 27.ix.46) showing strong x_G-ray used to determine an $N(h)$ profile.

Plate 2

Ionograms on night of 18.ix.46 (Hobart) showing features of an isolated occurrence of x_G-rays. Ionogram at 0030 shows a strong $(3F_2-2E_s)x_G$-ray.

Plate 3

Fig. 1.—Ionogram (Hobart, 0050, 5.xi.46) showing resolved frequency spreading above and below the gyro frequency.

Fig. 2.—Ionogram (Hobart, 0520, 6.ix.46) showing resolved range spreading above and below the gyro frequency.

Fig. 3.—Ionogram (Hobart, 0220, 11.vii.46) showing unresolved frequency spreading above and below the gyro frequency.

Fig. 4.—Ionogram (0250, 15.ii.48) showing an occurrence of x_G-rays at Brisbane.

SOME ASPECTS OF GYRO-SPLITTING IN THE IONOSPHERE

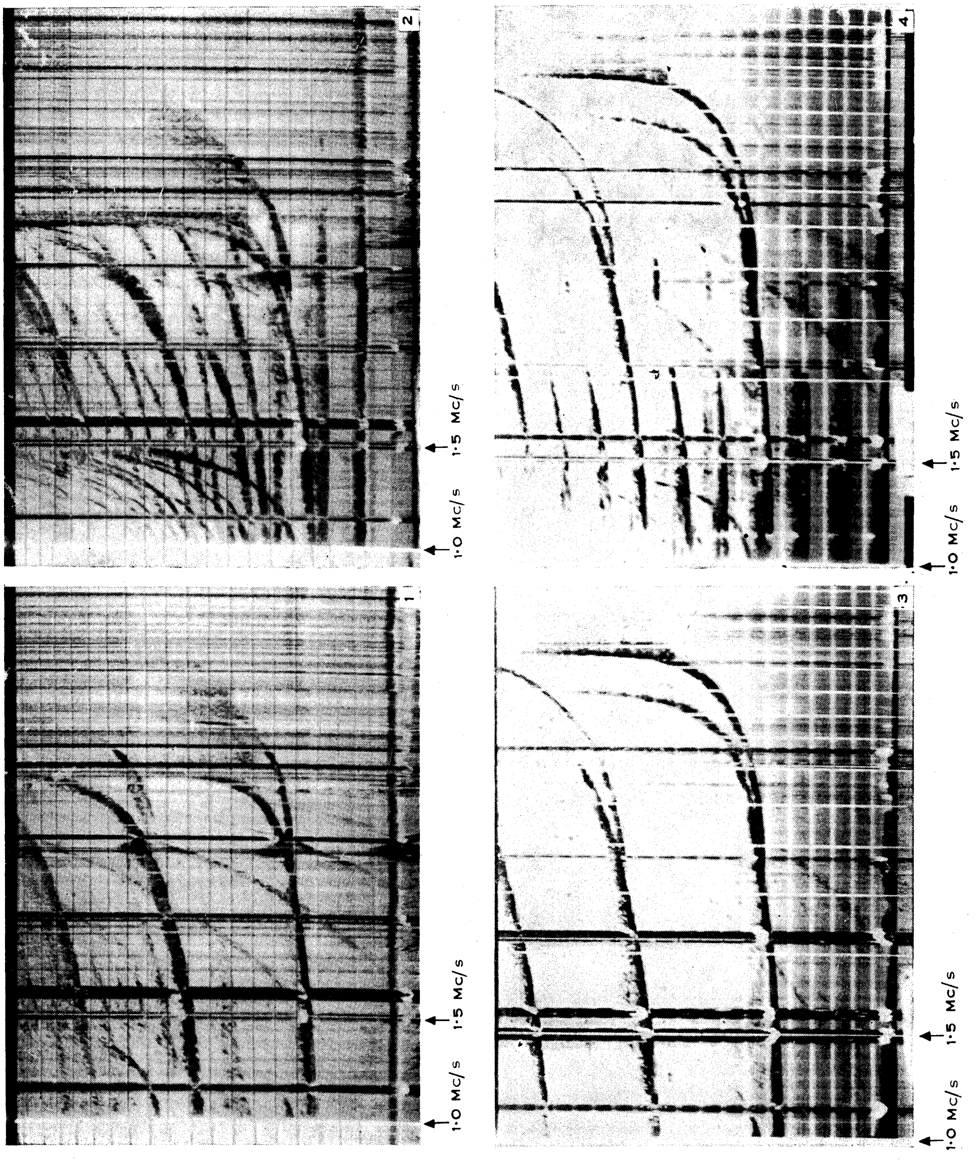

SOME ASPECTS OF GYRO-SPLITTING IN THE IONOSPHERE

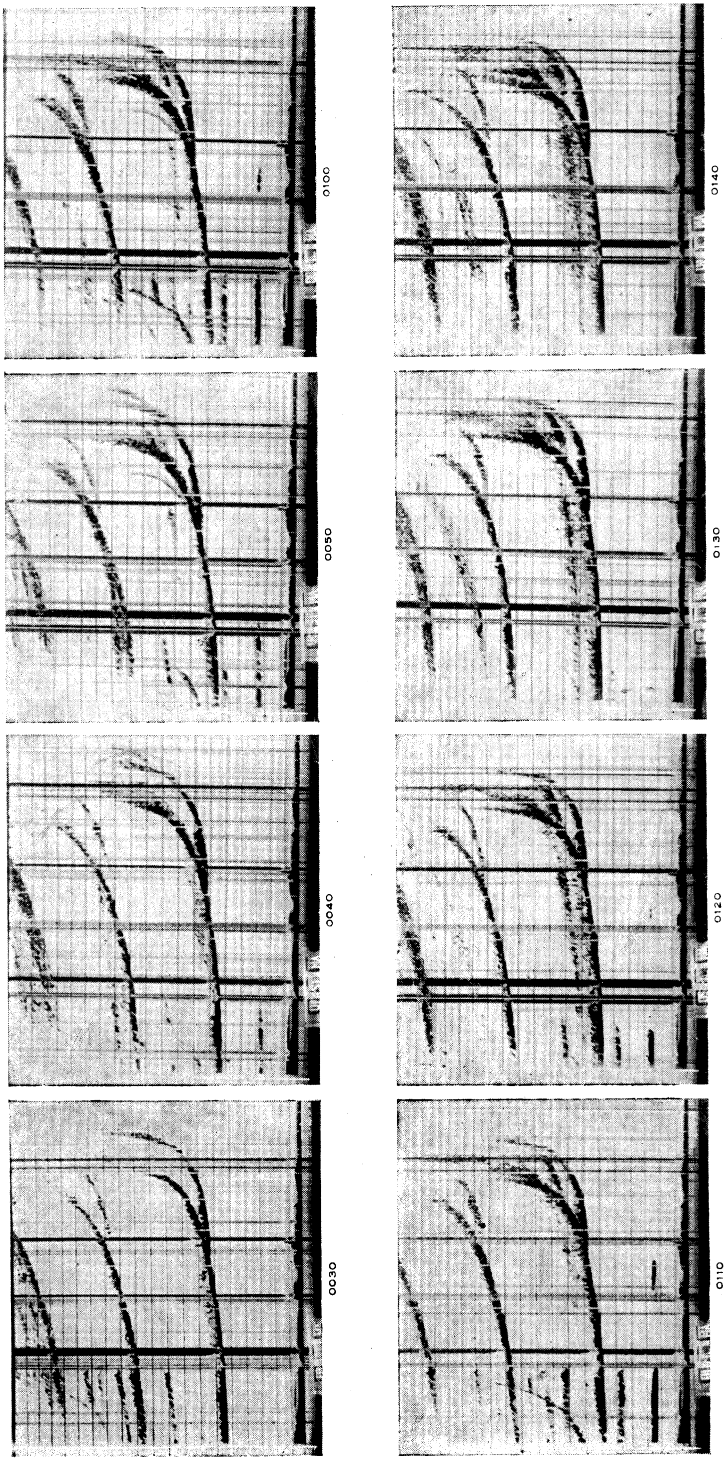

SOME ASPECTS OF GYRO-SPLITTING IN THE IONOSPHERE